J Mater Sci (2010) 45:3276–3283
DOI 10.1007/s10853-010-4339-1

Correlation between the morphology and photo-physical properties of P3HT:fullerene blends

David E. Motaung · Gerald F. Malgas · Christopher J. Arendse

Received: 30 October 2009 / Accepted: 19 February 2010 / Published online: 6 March 2010

Abstract The photo-induced charge transfer and opto-electronic efficiency of the solar cells correlated to the morphology and the structure of P3HT:C_{60} blend was studied by means of photoluminescence and electron spin resonance (ESR). The occurrence of photo-induced charge transfer, well-known for blends of P3HT with fullerenes, was evidenced in blends of P3HT:C_{60} (1:1 wt ratio) by a strong partially quenching of the P3HT luminescence. The ESR measurements allowed one to quantify the charge transfer between P3HT and C_{60}, which resulted in positive P3HT polarons. Wide-angle X-ray scattering (WAXS) and UV–vis spectroscopy showed that an inclusion of a C_{60} fullerene in the P3HT matrix lead to lower peak intensities and dark Debye rings and a blue shift on the π–π^* inter-band transition of the P3HT as well as a reduction in the absorption coefficient. Selected area electron diffraction patterns of a well-ordered sample of P3HT exhibit distinct diffraction rings indicating that the P3HT forms a poly-crystalline film. The large-scale phase separation of P3HT and C_{60} resulted from large C_{60} agglomerations during spin coating lead to a low power conversion efficiency of 0.2×10^{-4}%.

D. E. Motaung · G. F. Malgas (✉)
National Centre for Nano-Structured Materials, Council for Scientific and Industrial Research, P.O. Box 395, Pretoria 0001, South Africa
e-mail: gmalgas@csir.co.za

D. E. Motaung · C. J. Arendse (✉)
Department of Physics, University of the Western Cape, Private Bag X17, Bellville 7535, South Africa
e-mail: cjarendse@uwc.ac.za

Introduction

Since the discovery of charge separation in polymer/fullerene systems by Sariciftci et al. [1], organic photovoltaics became one of the most promising alternative concepts of solar cells based on crystalline silicon technology. This is due to their low cost, low temperature processing, flexibility and a very high speed of processing [2]. The technology of polymer photovoltaics has seen some drastic improvements in their power conversion efficiency with the introduction of the bulk heterojunction, consisting of an interpenetrating network of electron donor (D) and acceptor (A) materials [3, 4]. Power conversion efficiencies in the range of 6.5% have been achieved [5] successfully through selection of materials with suitable energy levels, control of nano-morphology [6] either during film deposition [7] or using post-fabrication procedures such as thermal annealing [8–14] and by optimisation of electrode materials [15].

Such progress makes polymer solar cells more competitive with amorphous silicon based solar cells. The main factors that limit the performance of polymer solar cells are charge carrier transport [16], narrow absorption in the visible range of the solar spectrum of the active layer and low open circuit voltages [17, 18]. In general, bicontinuous nanoscale morphology is pleasing for the D/A acceptor junctions, and high crystallinity in the D/A phases is also essential for better transportation ability of the charge carrier. However, the ideal bicontinuous two-phase nanoscale morphology is difficult to obtain due to the reduced solubility of the fullerene and inappropriate phase separation during the film cast process. Currently, several works have been reported on making nanorods or nanowires structures of P3HT or C_{60} to form a three-dimensional (3D) interpenetrating network such as the formation of fullerene

nanorod structures with different sizes by solvent–vapour treatments at different vapour pressures [19].

These approaches provide promising protocols for morphology manoeuvring of conjugated polymer/C_{60} for solar cells to obtain better charge carrier mobility and increase the absorption of solar energy. The C_{60} derivative; PCBM was mainly used in published works, due to its higher solubility. However, C_{60} may be a good candidate for an efficient acceptor material due to its higher electron mobility and crystalline structure compared to PCBM. The morphology fabrication of P3HT/C_{60} blends remains a fundamental challenge in the field of conjugated polymer/C_{60} solar cells [19, 20]. In this article, the photo-induced charge transfer and optoelectronic properties of photovoltaic cells correlated to the morphology and the structure of P3HT:C_{60} blend was studied in detail.

Experiment details

Materials

A regioregular poly (3-hexylthiophene) (rr-P3HT) polymer with a molecular weight (M_w) of $\sim$64,000 g mol^{-1}; with regularity that is greater than 98.5% for head-to-tail, buckminsterfullerene-C_{60} with a purity of 99.5%, indium tin oxide (ITO) coated on a 1-mm glass substrate with a sheet resistance of 8–12 Ω/sq^{-1}, poly (3,4-ethylenedioxythiophene):poly (styrenesulfonate) (PEDOT:PSS), and a chloroform ($CHCl_3$) solution were purchased from Sigma–Aldrich.

Sample preparation

All materials used in this study were used as received, without any further purification. Regioregular P3HT was used as an electron donor material; while a fullerene-C_{60} was used as an electron acceptor material. A mixture of rr-P3HT (5 mg) and C_{60} (5 mg) dissolved in 1 mL of $CHCl_3$ solution was stirred over night at a temperature of 50 °C in order to promote a complete dissolution. It should be noted that the solubility of C_{60} fullerene on chloroform is about 0.16 mg/mL [21].

For solar cells fabrication, a thin layer of PEDOT:PSS solution was spin coated onto the ultrasonically cleaned ITO glass substrates and silicon (Si) substrates with the spin rate of 2,500 rpm for 30 s. This was followed by thermal treatment of the substrates at 100 °C for 30 min. The P3HT and blends with a thickness of about 100 nm were spin coated onto the PEDOT:PSS layer. The spinning rate and time of spin coating were 2,500 rpm and 30 s, respectively. The samples were dried on a hot plate at a temperature of 50 °C for 15 min to dry (or evaporate) the excess solvent. Solar cells were completed by evaporating about 100 nm of aluminium (Al) on top of the active layer (ITO/P3HT:C_{60} (1:1 wt ratio)/Al) through a shadow mask by means of thermal evaporation in vacuum at a pressure of about 5×10^{-4} Pa resulting in an active device area of 0.14 cm^2.

Characterisation

Surface morphological studies of P3HT and P3HT:C_{60} (1:1 wt ratio) were carried out using an atomic force microscope (AFM) and a LEO 1525 SEM, operated at an accelerating voltage of 5 kV. The AFM images of the polymer films were acquired using a Veeco NanoScope IV Multi-Mode AFM with the tapping mode. A JEM-2100 JEOL high-resolution transmission electron microscope (HR-TEM), operated at 100 kV was employed to examine the internal structure of the P3HT and the blends. Specimens for HR-TEM analysis were prepared by a placing a drop of P3HT dispersed in $CHCl_3$, onto a holey-carbon copper (Cu) grid and dried at ambient conditions. In order to determine the structural modification during heating; wide-angle X-ray scattering (WAXS) measurements were performed using an Anton-Paar SAXSess instrument, operating at an accelerating voltage of 40 kV and current of 50 mA. A nickel (Ni) filtered CuK_α radiation source (0.154 nm) (PW3830 X-ray generator PANanalytical) radiation was used. Intensity profiles were obtained with a slit collimated compact Krathy Camera and recorded with a two-dimensional (2-D) imaging plate. Sample to detector distance was 264.5 mm and covers the length of the scattering angle (2θ) from 0.1 to 30°. The samples were heated in a paste cell at room temperature (RT) and 110 °C by a TCU50 (Anton-Paar) temperature control unit, which is attached to the SAXSess instrument.

The optical absorption study of spin-coated films was investigated by means of PekinElmer Lamda 750S Ultraviolet–visible (UV–vis) spectrophotometer. The photoluminescence (PL) measurements were carried out at RT by exciting the samples with the 350 nm deuterium lamp. The emission was detected with Jobin–Yvon PMT detector. It should be noted that for some PL measurements, the PEDOT:PSS layer was omitted in order to avoid masking of P3HT features, which overlap with those of PEDOT. The film thickness was determined by α-stepper DEKTAK 6M Stylus profilometer (Veeco instruments). Electron spin resonance (ESR) measurements were performed with a JEOL, X-band spectrometer JES FA 200 equipped with an Oxford ESR900 gas-flow cryostat and a temperature control (Scientific instruments 9700). Measurements were done at RT (23 °C). The power of 6.0 mW and frequency of 9.46 GHz were used.

The current density–voltage (J–V) characteristics of the polymer-based organic solar cells were measured both in the dark and under illumination using a Keithley 2420. The devices were irradiated at 100 mW cm^{-2} using a xenon lamp-based Sciencetech SF150 150 W solar simulator equipped with an AM1.5 filter as the white light source; the optical power at the sample was 100 mW cm^{-2}, detected using a daystar meter. All the photovoltaic properties were evaluated in ambient air conditions at RT. The solar cells were illuminated through the side of the ITO-coated glass plate.

Results and discussion

The morphology of polymer/fullerene photo-active layers that plays a key role in the final solar cell performance was investigated using scanning electron microscopy (SEM) analysis. Figure 1 shows the SEM micrographs of the surface of P3HT and blended films spin coated from a $CHCl_3$ solvent onto a silicon substrate. It is evident in Fig. 1a that the P3HT film shows a less-ordered morphology with pores uniformly across the film surface. A smooth surface for the P3HT film prepared from pyridine–chloroform solution was observed by Verma and Dutta [22]. The micrograph in Fig. 1b shows that the surface has clusters/agglomerates of C_{60} fullerene in the polymer matrix, which is uniformly distributed across the surface.

It is suggested that these clusters are nucleation sites, which could act as conduction pathways for charge carrier transport in the polymer phase and reduces the distance travelled by excitons to the respective polymer/C_{60} interface, which greatly enhances the effectiveness of photo-induced charge transfer from the polymer to C_{60}. Large agglomerated nanotubes in a P3HT film blended with a non-functionalized single-walled carbon nanotubes (non-FSWCNTs–P3HT) were observed by Kumar et al. [23].

To complement the HR-SEM analysis, AFM measurements were performed on the samples. Figure 2 presents the AFM height images of P3HT and blended film of P3HT:C_{60} in a 1:1 wt ratio. It is clear in Fig. 2a that pores with diameters ranging from 70–100 nm and lengths/depth that ranges between 3.5 and 9.0 nm are observed. A series of small clusters is observed in the P3HT:C_{60} blended film (Fig. 2b), which may be attributed to the C_{60} aggregates. The surface of P3HT and P3HT:C_{60} (1:1 wt ratio) films shows a root mean square (rms) roughness of 2.19 and 4.20 nm, respectively. It has been reported that the D/A blend morphology can be controlled by spin-casting the blend from a specific solvent preventing large-size phase separation or enhancing the polymer chain packing [6, 24].

High-resolution TEM was used to further study the details of ordering of the P3HT active layer as shown in Fig. 3. The inset in Fig. 3a corresponds to the (200) reflection, with a d-spacing of 0.86 nm. The selected area electron diffraction (SAED) pattern (Fig. 3b) of a well-aligned sample of P3HT exhibits distinct diffraction rings (spots) indicating that the P3HT forms a polycrystalline film. The P3HT structure shows the (100), (300) and (010) reflections, with a d-spacing of 1.73, 0.52 and 0.37 nm, respectively, which are consistent with the WAXS results.

The microstructure and domain spacing for P3HT and its blends were examined using WAXS technique. Representative WAXS patterns for the as-prepared P3HT and its blended samples measured at RT and heated at 110 °C are presented in Figs. 4 and 5. It is noticeable in Figs. 4 and 5 that P3HT depicts its characteristic peaks at $2\theta \approx 5.2°$, 10.7°, 16.3° and 23.4° at RT, with broadly bright Debye rings of (*h00*) assigned to (100), (200) (300) and (010) reflections [25].

The P3HT:C_{60} (1:1 wt ratio) blend in Figs. 4 and 5c, d shows low peak intensities and diffused Debye rings of (100) and (010) crystalline reflections assigned to P3HT and (111), (220), (311) assigned to C_{60} fullerene. This

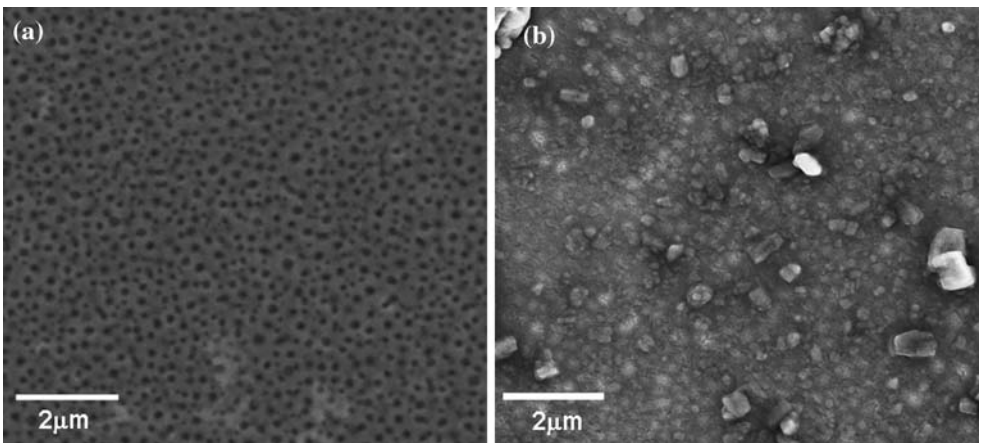

Fig. 1 SEM micrographs of the surface morphology of **a** P3HT and **b** blended film showing a dispersed C_{60} fullerene on the P3HT matrix

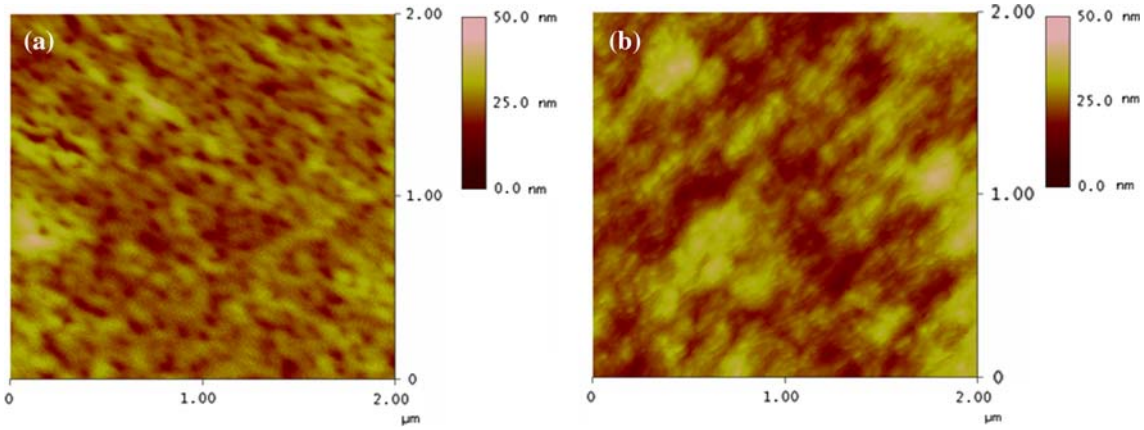

Fig. 2 AFM height images of P3HT and blended (1:1 wt ratio) films spin coated onto Si substrates

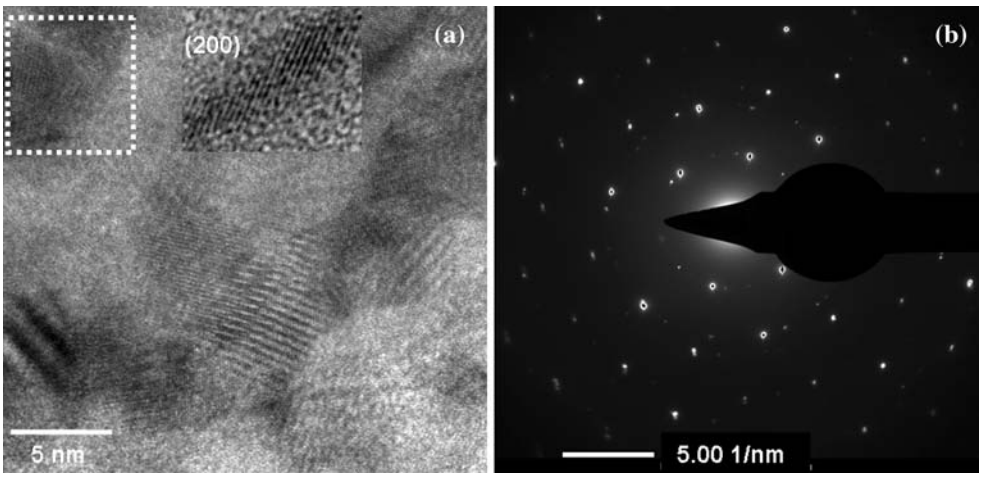

Fig. 3 HR-TEM images of **a** P3HT dissolved in $CHCl_3$ solution and **b** SAED pattern of the P3HT

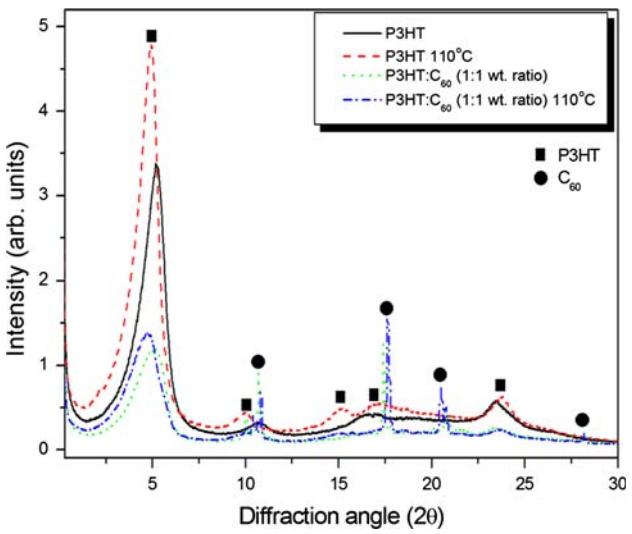

Fig. 4 Wide-angle X-ray scattering patterns measured at RT and 110 °C of P3HT and its blend

indicates that the blended sample has a low crystallinity and less-ordered crystal orientation than a pure P3HT sample. The intensity of the (100) reflection, due to lamella layer structure (1.64 nm), is strong, while the intensity of the (010) reflection due to π–π interchain stacking (0.38 nm) is very weak [26].

The C_{60} diffraction patterns (Fig. 5e, f) are consistent with results obtained for buckminsterfullerene [25, 27–29], which is known to have a face-centred-cubic (fcc) crystal structure at RT, and shows reflections for the (111), (220), (311), (222) and (331) diffraction peaks at 10.6°, 17.7°, 20.9°, 21.7° and 27.4°, respectively [25, 27–29]. From the WAXS patterns of P3HT and the blended sample, the *d*-spacing ranges between 0.37 and 1.96 nm, and were estimated using Bragg's law [30], while the crystal sizes were estimated using Scherrer's relation [31] as shown in Table 1.

However, when the P3HT sample is heated at a temperature of 110 °C, diffraction peaks shift to lower angles

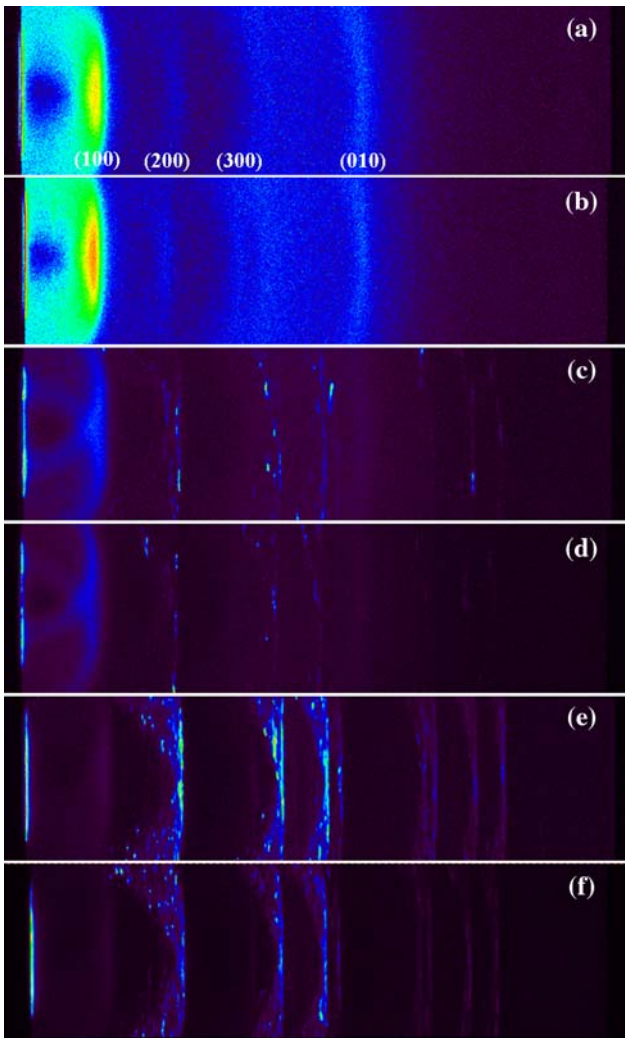

Fig. 5 2-D wide-angle X-ray scattering patterns of: **a** P3HT at RT, **b** P3HT at 110 °C, **c** P3HT:C_{60} (1:1 wt ratio) at RT, **d** 1:1 wt ratio at 110 °C, **e** fullerene C_{60} at RT and **f** C_{60} at 110 °C

($2\theta \approx 4.7°, 9.8°$ and 16.0°), giving a significant increase in *d*-spacing and grain sizes of the (100) plane, as depicted in Table 1. This indicates an increase in the ordering of the alkyl chains within the main thiophene chains. It is interesting to note that at 110 °C a broad peak formed around 17.1° with a d-spacing and crystal size of 0.51 and 1.99 nm, respectively (Fig. 4). The formation of this peak is clear in Fig. 5b as indicated by an arrow.

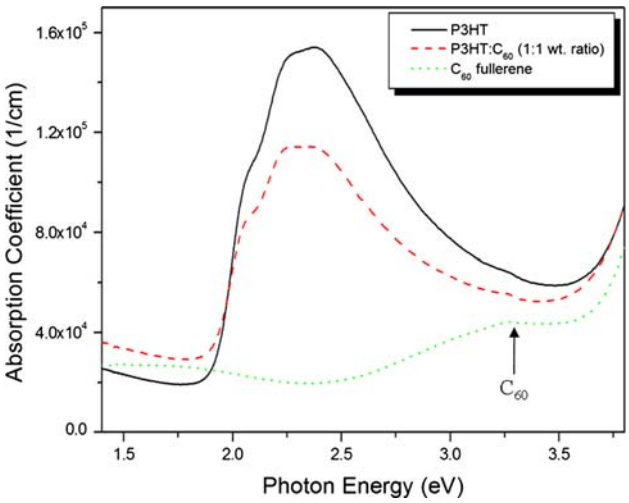

Fig. 6 UV–vis spectra of films of P3HT, P3HT:C_{60} (1:1 wt ratio) blend and C_{60} fullerene dissolved in $CHCl_3$ and spin coated on ITO substrates

Figure 6 compares the optical absorption coefficient spectra of rr-P3HT films with C_{60} fullerene and a blend of P3HT:C_{60} in a (1:1 wt ratio) spin coated on an ITO glass substrate. Both polymers showed the band gap edge at 1.9 eV, which is in agreement with the literature [32–35], and an absorption maximum at around 2.4 eV, which is characteristic of the π–π^* transition between the highest occupied π electron band and the lowest unoccupied one of the polymer [36].

The development of a vibronic structure is also observed (refer to the shoulders peak around 2.25 and 2.06 eV), which is generally explained by a higher crystallization or ordering of intra-chain interactions in semiconducting polymers [37, 38]. The C_{60} fullerene shows a small absorption peak at around 3.31 eV. Upon blending the polymer with a C_{60} fullerene, a distinctive change in the peak wavelength is observed.

A blue shift on the π–π^* interband transition of the P3HT blend as well as a reduction in the absorption coefficient is observed [35]. This is probably due to an altering in the stacking conformation of the polymer structure and a reduction of the intraplane and interplane stacking, which causes a reduced π–π^* transition and a lower absorbance (Fig. 6). Chirvase et al. [39] reported that

Table 1 Summary of the full width and half maximum, *d*-spacing and grain sizes of the as-prepared rr-P3HT and samples heated at 110 °C

Orientations	As-prepared P3HT			P3HT (110 °C)		
	d-spacing (nm)	FWHM (nm)	Grain sizes (nm)	*d*-spacing (nm)	FWHM (nm)	Grain sizes (nm)
(100)	1.70	1.38	5.80	1.87	1.26	6.32
(200)	0.83	1.41	5.73	0.90	1.01	7.99
(300)	0.54	3.60	2.29	0.55	2.49	3.32
(010)	0.38	1.53	5.66	0.37	1.25	6.94

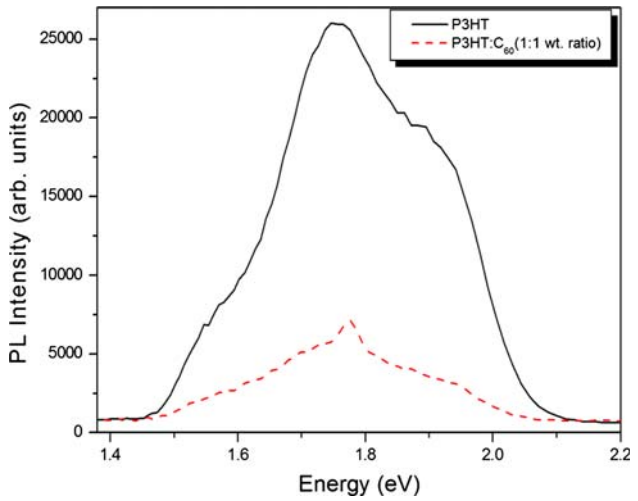

Fig. 7 Photoluminescence spectra of films of P3HT and P3HT:C_{60} (1:1 wt ratio) dissolved in $CHCl_3$ and measured at room temperature

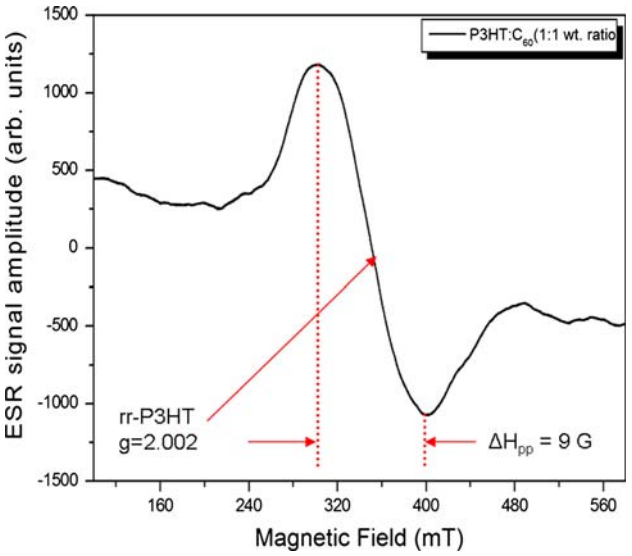

Fig. 8 ESR spectra of the P3HT and blend films extracted at the power of 6.0 mW (microwave power) in the dark

the modification in the absorption spectra of P3HT:PCBM composite films are due to the presence of PCBM, which destructs the ordering in the P3HT chains.

Photoluminescence measurements were carried out extensively to evaluate the effectiveness of the photo-induced charge transfer in an electron donor–acceptor pair. The PL spectra of P3HT and its blend with C_{60} fullerene measured at RT are shown in Fig. 7. The P3HT film shows a strong PL signal around 1.75 eV and a shoulder around 1.92 eV, which are assigned to the first vibronic band and the pure electronic transition, respectively [40–43]. The PL emission peak in the shorter energy region ($\sim$1.55 eV) indicates an ordering in the P3HT lamella structure within the spherulites [40–43]. It is evident in Fig. 7 that when fullerene is added in the P3HT matrix, the intense PL of the P3HT is almost completely quenched. The luminescence studies indicate a profound photoinduced charge transfer in the bulk of P3HT:C_{60} (1:1 wt ratio) blended film.

The effective charge separation in the P3HT:C_{60} (1:1 wt ratio) system has been studied by ESR signals. The spectrum of the blended film shown in Fig. 8 was extracted at a microwave power of 6.0 mW in the dark at RT. A large ESR signal caused by a partial charge transfer is observed between rr-P3HT and fullerene in the dark state [44, 45]. Only rr-P3HT signals can be observed at RT, due to the short spin-relaxation time for the C_{60} anions. The g-factor of the P3HT sample is about 2.0020, which can be attributed to the positive polarons in P3HT (P^+). These results are in good agreement with that obtained in the literature [46, 47]. A peak-to-peak line width ($\Delta H_{pp} = 9$ G) is observed for the blend. This indicates that rr-P3HT orientation is disturbed [48], caused by the incomplete mixing of C_{60} as shown in the SEM (Fig. 1b). More detailed discussion, however, is beyond the scope of this work.

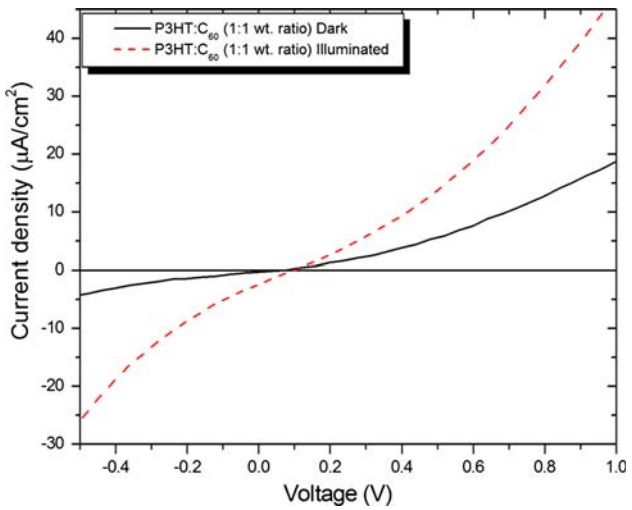

Fig. 9 Current density–voltage (J–V) characteristics of P3HT:C_{60} (1:1 wt ratio) measured in the dark and under white light illumination

Figure 9 presents the current density–voltage (J–V) characteristics of a P3HT:C_{60} (1:1 wt ratio) device measured in the dark and under AM1.5 conditions with a white light illumination. The device achieved a short-circuit current density (J_{sc}) of 2.55 μA cm^{-2}, an open circuit voltage (V_{oc}) of 0.092 V, the fill factor of 0.20 and a final power conversion efficiency of about 0.2×10^{-4}%. The low V_{oc}, J_{sc} and efficiency may be attributed to the formation of large-size C_{60} crystals (Fig. 1), which causes not only a large-scale phase separation between P3HT and C_{60}, but also a rough P3HT:C_{60} (1:1 wt ratio) blend film as depicted in Fig. 2. The rough P3HT:C_{60} layer may form some shunt paths after the top electrode deposition, resulting in a low open circuit voltage.

Moulé et al. [49] reported that the morphology of the active layer strongly influences the performance of bulk heterojunction (BHJ) polymer solar cells. Previous studies of polycrystalline perylene diimide films have demonstrated exciton diffusion lengths of up to 2.5 μm [50]. However, the exciton diffusion length in conjugated polymers is merely about 10 nm, which are several orders of magnitude smaller than that in perylene diimide polycrystals. Therefore, the large phase separation of P3HT:C_{60} blend device might causes inefficient charge separation of excitons created in P3HT, due to its short diffusion lengths.

Conclusion

In conclusion, we investigated the photo-induced charge transfer correlated to the morphology and the structure of P3HT:C_{60} blended organic solar cells. The occurrence of photo-induced charge transfer was evidenced in blends of P3HT:C_{60} (1:1 wt ratio) by a strong partially quenching of the P3HT luminescence. The ESR measurements allowed one to quantify the charge transfer between P3HT and C_{60}, which resulted in positive P3HT polarons. WAXS data and UV–vis spectroscopy showed that an incorporation of C_{60} in P3HT matrix lead to lower peak intensities, dark Debye rings and a blue shift on the π–π^* interband transition of the P3HT as well as a reduction in absorption coefficients. The shift in diffraction peaks to lower angles, giving a significant increase in *d*-spacing and grain sizes of the (100) plane for films evaluated at 110 °C was observed. The large-scale phase separation of P3HT and C_{60} resulted from large C_{60} agglomerations during spin coating, as observed by AFM and SEM, lead to a low power conversion efficiency of 0.2×10^{-4}%.

Acknowledgements The authors would like to thank the financial support of the Department of Science and Technology (DST), the Council for Scientific and Industrial Research (CSIR, Project No. HGERA7S), and the National Research Foundation (NRF) of South Africa. The authors are also grateful to Mrs. Jayita Bandyopadhyay and Mr. Thomas Malwela for their help and assistance with the small angle x-ray scattering and atomic force microscopy analysis.

References

1. Sariciftci NS, Smilowitz L, Heeger AJ, Wudl F (1992) Science 258:1474
2. Bundgaard E, Krebs FC (2007) Sol Energy Mater Sol Cells 91:954
3. Yu G, Gao J, Hummelen JC, Wudl F, Heeger AJ (1995) Science 270:1789
4. Shaheen SE, Ginley DS, Jabbour GE (2005) MRS Bull 30:10
5. Kim JY, Lee K, Coates NE, Moses D, Nguyen Thuc-Quyen, Dante M, Heeger AJ (2007) Science 317:222
6. Shaheen SE, Brabec CJ, Sariciftci NS, Padinger F, Fromherz T, Hummelen JC (2001) Appl Phys Lett 78:841
7. Li G, Shortriya V, Huang J, Yao Y, Moriarty T, Emery K, Yang Y (2005) Nat Mater 4:864
8. Ma WL, Yang CY, Gong X, Lee KH, Heeger AJ (2005) Adv Funct Mater 15:1617
9. Padinger F, Ritterberger RS, Sariciftci NS (2003) Adv Funct Mater 13:85
10. Kim Y, Choulis SA, Nelson J, Bradley DDC, Cook S, Durrant JR (2005) Appl Phys Lett 86:063502
11. Kim Y, Cook S, Tuladhar SM, Nelson J, Durrant JR, Bradley DDC, Giles M, McCulloch I, Ree M, Ha CS (2006) Nat Mater 5:197
12. Ko CJ, Lin YK, Chen FC (2007) Adv Mater 19:3520
13. Reyes-Reyes M, Kim K, Dewald J, López-Sandoval R, Avadhanula A, Curran S, Carroll DL (2005) Org Lett 7:5749
14. Peumans P, Uchida S, Forrest SR (2003) Nature 425:158
15. Irwin MD, Buchholz DB, Hains AW, Chang RPH, Marks TJ (2008) Proc Natl Acad Sci 105:2783
16. Wang WL, Wu HB, Yang CY, Luo C, Zhang Y, Chen JW, Cao Y (2007) Appl Phys Lett 90:183512
17. Loi MA, Toffanin S, Muccini M, Forster M, Scherf U, Scharber M (2007) Adv Funct Mater 17:2111
18. Chen CP, Chan SH, Chao TC, Ting C, Ko BT (2008) J Am Chem Soc 130:12828
19. Lu G, Li L, Yang X (2008) Small 4:601
20. Yang XN, Lu GH, Li LG, Zhou EL (2007) Small 3:611
21. Ruoff RS, Tse DS, Malhotra R, Lorents DC (1993) J Phys Chem 97:3379
22. Verma D, Dutta V (2009) J Renew Sustain Energy 1:023107
23. Kumar J, Singh RK, Kumar V, Rastogi RC, Singh R (2007) Diam Relat Mater 16:446
24. van Duren JKJ, Yang X, Loos J, Bulle-Lieuwma CWT, Sieval AB, Hummelen JC, Janssen RAJ (2004) Adv Funct Mater 14:425
25. International Centre for Diffraction Data (ICDD): P3HT (48-2040), C_{60} fullerene (47-0787, 44-0558)
26. Prosa TJ, Winokur MJ, Moulton J, Smith P, Heeger AJ (1992) Macromolecules 25:4364
27. Heiny PA, Fischer JE, McGhie AR, Romanow WJ, Denenstein AM, Jr McCauley JP, Smith ABIII, Cox DE (1991) Phys Rev Lett 66:2911
28. Cagiao ME, Pozdnyakov AO, Krumova M, Kudryavtsev VV, Balta Callej F (2007) J Compos Sci Technol 67:2175
29. Li JQ, Zhao ZX, Li YL, Zhu DB, Gan ZZ, Yin DL (1992) Physica C 196:135
30. Warren BE (1990) X-ray diffraction. Dover, New York, p 251
31. Cullity BD (1978) Elements of X-ray diffraction, 2nd edn. Addison-Wesley Publishing Co., Reading, MA
32. Ahn T, Choi B, Ahn SH, Han SH, Lee H (2001) Synth Met 117:219
33. Dicker G, Savenije TJ, Huisman B-H, de Leeuw DM, de Haas MP, Warman JM (2003) Synth Met 137:863
34. Apperloo JJ, Janssen RAJ, Nielsen MM, Bechgaard K (2000) Adv Mater 12:1594
35. Salaneck WR, Lundstrom I, Ranby B (eds) (1993) Conjugated polymers and related materials proceedings of the eighty-first nobel symposium. Oxford University Press, Oxford, p 290
36. Jiang X, Osterbacka R, Korovyanko O, An CP, Horowitz B, Janssen RAJ, Vardeny ZV (2002) Adv Funct Mater 12:587
37. Brown PJ, Thomas DS, Kohler A, Wilson JS, Kim JS, Ramsdale CM, Sirringhaus H, Friend RH (2003) Phys Rev B 67:064203
38. Chung TC, Kaufman JH, Heeger AJ, Wudl F (1984) Phys Rev B 30:702
39. Chirvase D, Parisi J, Hummelen JC (2004) Nanotechnology 15:1317

40. Sharma M, Kaushik D, Singh RR, Pandey RK (2006) J Mater Sci Mater Electron 17:537
41. Motaung DE, Malgas GF, Arendse CJ, Mavundla SE, Knoesen D (2009) Mater Chem Phys 116:279
42. Li L, Chan C-M, Yeung KL, Li J-X, Ng K-M, Lei Y (2001) Macromolecules 34:316
43. Yang H, Shin T, Yang JL, Cho K, Ryu CY, Bao Z (2005) Adv Funct Mater 15:671
44. Marumoto K, Takeuchi N, Kuroda S (2003) Chem Phys Lett 382:541
45. Marumoto K, Takeuchi N, Ozaki T, Kuroda S (2002) Synth Met 129:239
46. Dietmueller R, Stegner AR, Lechner R, Niesar S, Pereira RN, Brandt MS, Ebbers A, Trocha M, Wiggers H, Stutzmann M (2009) App Phys Lett 94:113301
47. Marumoto K, Muramatsu Y, Nagano Y, Iwata T, Ukai S, Ito H, Kuroda S, Shimoi Y, Abe S (2005) J Phys Soc Jpn 74:3066
48. Watanabea S, Tanaka H, Ito H, Marumoto K, Kuroda S (2009) Synth Met 159:893
49. Moulé AJ, Meerholz K (2008) Adv Mater 20:240
50. Dittmer JJ, Marseglia EA, Friend RH (2000) Adv Mater 12:1270